ARTICLE NO. 78-1202R

Aerodynamics of Strake-Wing Interactions

James M. Luckring*
NASA Langley Research Center, Hampton, Va.

This paper reports on an experimental investigation where the longitudinal aerodynamic characteristics were determined up to high angles of attack for configurations employing parametric variations in strake span and wing sweep and includes correlations with theory. The investigation included both component and complete configuration studies to provide information for the analysis of interaction effects. Comparisons between strake-wing and high canard-wing configurations demonstrate the strake wing to develop higher lift coefficients than did the canard wing due to enhanced interference effects. Correlations with theory demonstrate the suction analogy to be a useful method for estimating the effects of vortex flow aerodynamics on both component and total forces and moments.

Nomenclature

A = aspect ratio, b^2/S_{ref}
b = wing reference span, 50.80 cm (20.00 in.)
C_D = drag coefficient, drag/$q_\infty S_{ref}$
ΔC_D = drag due to lift coefficient, drag due to lift/$q_\infty S_{ref}$
C_L = lift coefficient, lift/$q_\infty S_{ref}$
ΔC_L = increment in lift due to strake, C_L (strake on) − C_L (strake off)
C_m = pitching moment coefficient, pitching moment/$q_\infty S_{ref}\bar{c}$
c = streamwise chord
c_s = section suction-force coefficient, section suction force/$q_\infty c$
c_t = section thrust-force coefficient, section thrust force/$q_\infty c$
$\bar{c}$ = reference chord, 23.33 cm (9.184 in.)
$\bar{c}$ = characteristic length used in determination of $K_{v,\overline{se}}$
f = additional lifting surface efficiency factor (see Fig. 12)
$K_{v,le}$ = leading-edge vortex lift factor, ∂[(leading-edge suction force)/$q_\infty S_{ref}$]/$\partial \sin^2\alpha$
$K_{v,se}$ = side-edge vortex lift factor, ∂[(side-edge suction force)/$q_\infty S_{ref}$]/$\partial \sin^2\alpha$
$K_{v,\overline{se}}$ = augmented vortex lift factor
l = length
M_∞ = freestream reference Mach number
q_∞ = freestream dynamic pressure, Pa (lbf/ft^2)
R_a = S_a/S_{ref}
S = exposed area
S_a = exposed area of strake or canard
S_{ref} = reference wing area—wing leading and trailing edges extended to centerline, 1032 cm^2 (159.970 in.^{2})
α = angle of attack
Λ = leading-edge sweep angle

Subscripts

inbd = inboard
max = maximum
outbd = outboard
p = potential
s = strake
te = trailing edge
tot = total
v = vortex
w = wing

All coefficients refer to total loads unless stated otherwise. The subscript "tot" is selectively used for cases where confusion might occur.

Introduction

THE close-coupled strake-wing concept has received considerable attention in recent years as a means of enhancing the high-α aerodynamic characteristics of maneuvering aircraft. The enhanced maneuver aerodynamics are primarily due to the formation of strong vortices along the leading and side edges of the strake. In addition to producing large vortex lift increments on the strake itself, these vortices persist over the wing and provide favorable induced effects to the wing flowfield resulting in additional lift increments. However, the persistence of the strake vortex over the wing, as well as the relative proximity of the wing and strake, results in a very complex flow, characterized not only by closely coupled strake-wing aerodynamics but also by multiple regions of separation-induced vortex flow. Because of these flow complexities, as well as the comparatively recent interest in strake-wing geometries, very little parametric information is available on this topic for use in future advanced configuration studies. To this end, parametric wind-tunnel investigations have been undertaken to help establish a data base for both longitudinal[1] and lateral-directional[2] aerodynamic characteristics of strake-wing configurations up to high α's. The longitudinal experimental investigation was conducted in the Langley 7 × 10 ft tunnel at Mach numbers ranging from 0.3-0.8; the angle of attack ranged from approximately 0-50 deg at zero sideslip.

This paper presents a summary of the $M = 0.3$ experimental results of Ref. 1 and includes correlations with theory. The experimental investigation included both component and complete configuration studies to provide information for the analysis of interaction effects. In addition to comparisons between various strake-wing geometries, comparisons are made between strake-wing and canard-wing configurations. The theoretical analysis was accomplished using the suction analogy of Polhamus[3-5] to account for the leading-edge

Presented as Paper 78-1202 at the AIAA 11th Fluid and Plasma Dynamics Conference, Seattle, Wash., July 10-12, 1978; submitted Sept. 11, 1978; revision received May 11, 1979.

Index category: Aerodynamics.

*Aeronautical Research Engineer. Member AIAA.

vortex lift effects and included the effects of side-edge separation on vortex lift estimates.[6] The effects of the strake vortex persisting over the wing were modeled by the concept of augmented vortex lift.[7,8]

Model Description

A general model drawing is presented in Fig. 1. This model was originally designed so that various wing and canard planforms could be attached to a common fuselage and has been used for many parametric studies.[9-15] The model was instrumented with two internally mounted strain-gage balances. One balance, referred to as the strake balance, measured loads on the strake and the forebody (see shaded portion of Fig. 1) and the other balance, referred to as the main balance, measured total loads. The difference between the main and strake balance measurements would, therefore, be the loads on the wing and afterbody. To prevent fouling of the strake balance, a small gap was maintained between the forebody-strake and afterbody-wing segments of the model. Noninterfering wiper seals were rigidly attached to the lower surface of the forebody strake and allowed to lap over the gap to prevent air from bleeding through the gap.

The parameters altered for the present investigation were strake span and wing sweep (Fig. 2). The five different wings that were tested, designated wings I-V, had leading-edge sweep angles of 30, 40, 44, 50, and 59.45 deg, respectively. All wings had the same area, span, mean geometric chord, and airfoil section. The wings were untwisted and had biconvex airfoil sections which linearly varied in maximum thickness from 6% of the chord at the wing-fuselage juncture to 4% of the chord at the tip. The wings were mounted longitudinally at the same fuselage station and the quarter-chord point of the wing chord at the wing-fuselage juncture was taken as the moment reference point. All wings had a reference aspect ratio and taper ratio of 2.5 and 0.2, respectively.

The three strakes tested, designated strakes I, II, and III, had maximum exposed semispans of 10, 20, 30%, respectively, of the reference wing semispan. All strakes had the same root chord (at the strake-fuselage juncture) and had spanwise ordinates which were identical in percent maximum semispan (see Ref. 1). The strakes initially had a trailing-edge sweep angle equal to the leading-edge sweep angle of wing V. To accommodate the lower sweep wings, a portion of the strake near the trailing edge was removed such that the strake trailing edge sweep angle matched the wing leading-edge sweep angle. The strakes were flat plates which, in accordance with the purposes of this study, had sharply beveled leading and side edges to assure the strong formation of separation-induced vortex flows.

Experimental Results

Although measurements were obtained for the entire configuration matrix (including component configurations), this paper will focus on the characteristics of the configurations incorporating the 44 deg wing. Key aerodynamic quantities will be summarized as a function of strake span and/or wing sweep.

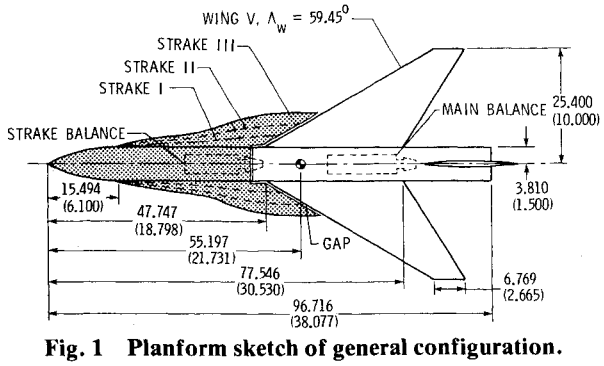

Fig. 1 Planform sketch of general configuration.

Aerodynamic Force Characteristics

Because the lifting surface had sharp edges, no camber, and high local sweep angles, the resultant aerodynamic characteristics can be characterized to various degrees by the separation-induced vortex flow phenomenon. Figure 3 presents typical surface flow patterns at 10 deg α for the configuration incorporating the large strake and either the 44 or 60 deg wing. These photographs clearly evidence both the strake and wing primary vortices and, in addition, show some secondary vortex effects. The longitudinal aerodynamic characteristics of the configurations incorporating these wings with the various strakes (as well as with no strake) are presented in Figs. 4-6. In Fig. 4, the parameters $C_{L,\max}$ and $(\Delta C_L)_{\max}$ are shown for the configuration incorporating the large strake with the 44 deg wing and will be used later to summarize planform effects. The addition of the various strakes to the 44 deg wing resulted in considerable increases in lift coefficient at moderate to high α's. Because the 60 deg wing is sufficiently swept to develop appreciable vortex lift, the increments in lift realized by adding the various strakes to this wing tended to be smaller than they had been for the 44 deg configurations, although the overall levels of lift are comparable.

Even though the strakes provide substantial lift increments at maneuver α's, it is of interest to note that they have very little influence on the lift characteristics at low α's (Fig. 4). The strake, therefore, provides a means to enhance the high-α maneuver aerodynamics without appreciably increasing the low-α gust response associated with the low-altitude dash.

The pitch characteristics of these same configurations (Fig. 5) show that an increase in strake span extended the linearity of the pitch curves to increased lift coefficients. However, the straked configurations exhibit the well-known pitch-up

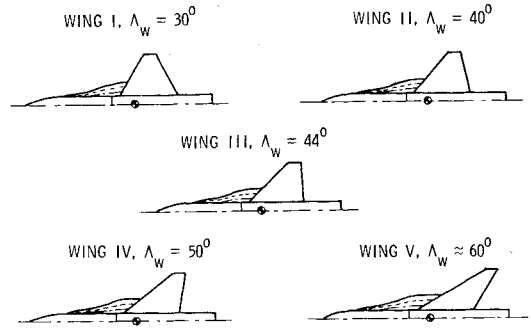

Fig. 2 Parametric variation of strake span and wing sweep.

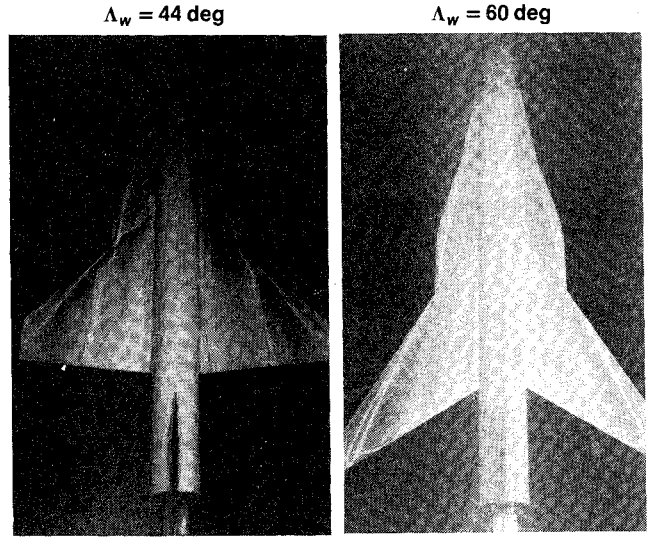

Fig. 3 Typical surface flow patterns, $\alpha \approx 10$ deg; $R_a \approx 0.27$.

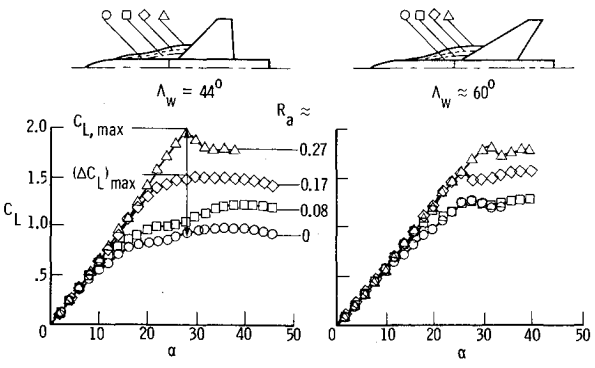

Fig. 4 Effect of strake span and wing sweep on lift characteristics.

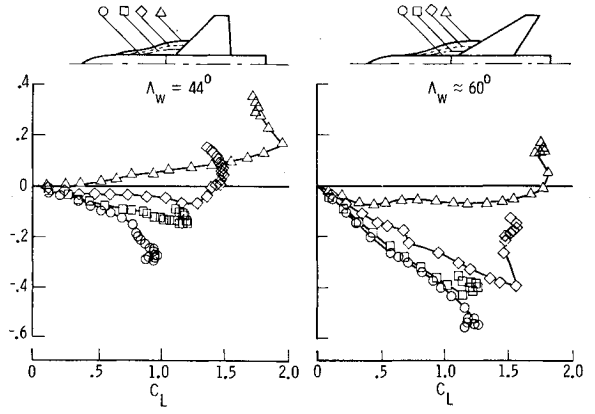

Fig. 5 Effect of strake span and wing sweep on pitching moment characteristics.

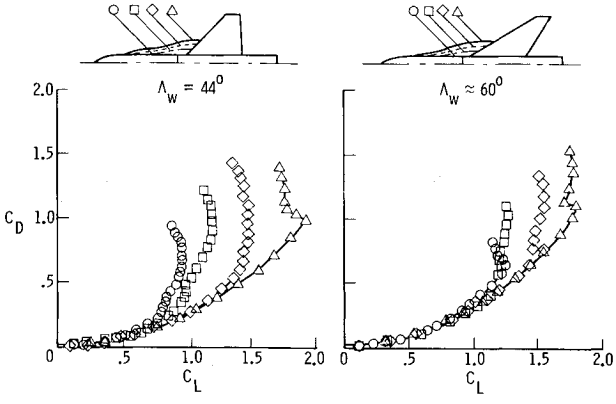

Fig. 6 Effect of strake span and wing sweep on drag characteristics.

tendency near $C_{L,max}$, whereas the wing-alone configurations exhibited stable characteristics. Figure 6 shows that the configurations incorporating the strakes maintained lower drag levels to higher lift coefficients as strake span was increased compared to the wing-alone configuration. The characteristics of the configurations incorporating the 44 deg wing are, in general, typical of the other configurations tested, but not discussed herein.

Figure 7 presents a comparison of the surface flow patterns at 30 deg α for the configurations employing the 44 deg wing with and without the large strake. Whereas the wing is essentially stalled for the strake-off configuration, it exhibits orderly vortex-flow patterns in the presence of the strake. The experimental trends discussed in this section primarily arise not only because of the vortex lift increments realized by the strake, but also due to the effects of the strake vortex on the wing aerodynamics.

Figure 8 summarizes the effects of strake span and wing sweep on the maximum lift coefficient, $C_{L,max}$. The symbols refer to the variation of strake span for the left portion and the variation of wing sweep for the right portion of this figure. For the configuration incorporating the 50 deg wing with the medium strake, the data, though repeatable, seem to be inconsistent with the other results and are shown as a dashed symbol. While the effects of wing sweep on $C_{L,max}$ were moderate for each strake, adding the strake to the wing caused the maximum lift coefficient to increase roughly three times as fast as the additional strake area did. Hence, beneficial interference effects are occurring for the strake-wing configuration much as has been the case for canard-wing configurations.[11-14]

Interaction Effects

In addition to the maximum lift coefficient, $C_{L,max}$, the maximum increment in lift coefficient due to the addition of a strake to a configuration, $(\Delta C_L)_{max}$, can be a useful summary parameter. This parameter is illustrated in Fig. 4 for the configuration employing the 44 deg wing with the large strake and is summarized in Fig. 9 for the configurations of the present investigation. The higher curves shown in Fig. 9 represent the total value of $(\Delta C_L)_{max}$ which seems to reach a maximum level in the vicinity of 44 deg wing sweep for all three strakes. The wings having leading-edge sweep angles greater than 44 deg developed higher levels of vortex lift and, hence, the increment in lift realized by adding a strake to these wings was less. (This point was also shown in Fig. 4.) The lower curves of Fig. 9 represent the increment in lift developed by the strake with the wing off at the α for which $(\Delta C_L)_{max}$ occurred. The difference between the upper and lower curves represents the interference lift which can be seen to be large when compared to the lift of the strake itself. It is interesting to note that the decrease in $(\Delta C_L)_{max}$ at the higher values of wing sweep angle seems to be due to a loss of interference lift.

These interference lift effects results in an aerodynamic synergism for strake-wing configurations much as has been observed for canard-wing configurations.[13] A comparative example of the synergistic effects is presented in Fig. 10 between a high canard[13] and a coplanar strake (present investigation) of approximately the same area, each in the presence of the same wing ($\Lambda_w = 44$ deg). The canard results of Ref. 13 are for the configuration which exhibited the maximum interference lift effects. The straked configuration developed higher lift coefficients than did the canard configuration between 15 deg and the α where vortex breakdown occurred; above this angle of attack the lift was comparable for both configurations. The component loads for the same configurations (Fig. 11) illustrate that the wing developed more lift in the presence of the strake than it did in the presence of the high canard. In addition, the strake developed more lift in the presence of the wing and more interference lift referenced to the wing-off case than did the canard. These combined effects demonstrated that the strake-wing concept of the present study was preferable to the canard-wing concept of Ref. 13 insofar as absolute (untrimmed) levels of lift are concerned, due to increased favorable interference effects. Because of the vortex flow, the drag due to lift for these flat wing configurations can be approximated as $\Delta C_D = C_L \tan\alpha$. The aforementioned interference lift effects result in the strake-wing configuration developing a given amount of lift at a lower α than the canard-wing configuration. As a consequence, the strake-wing configuration exhibited lower levels of drag due to lift than the canard wing.

To help quantify the interference lift effects, a parameter, referred to as the additional lifting surface efficiency factor, is introduced. This parameter accounts for the additional lifting surface area of the strake or canard and is defined as

$$f = \frac{(C_{L,tot})_{ws}}{(C_{L,tot})_w}\left(\frac{S_{ref}}{S_{ref} + S_a}\right) \quad (1)$$

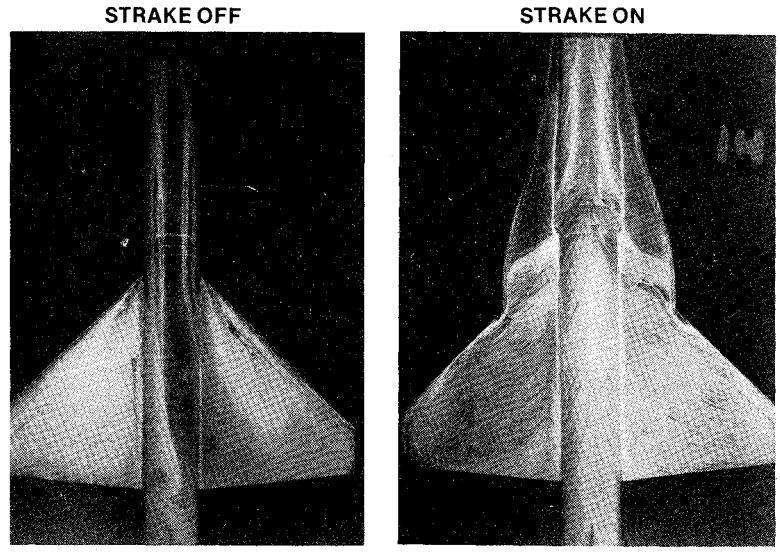

Fig. 7 Effect of strake on high angle of attack surface flow patterns $\alpha \approx 30$ deg, $R_a \approx 0.27$, $\Lambda_w = 44$ deg.

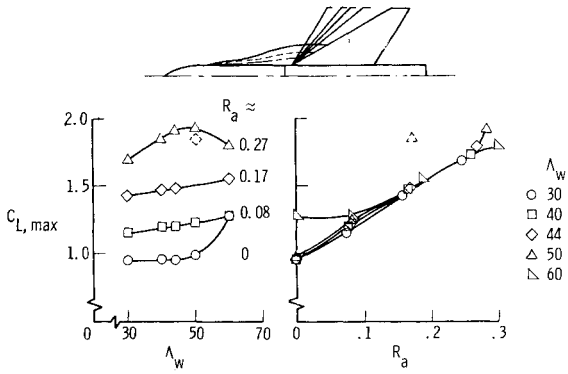

Fig. 8 Effect of strake span and wing sweep on $C_{L,max}$.

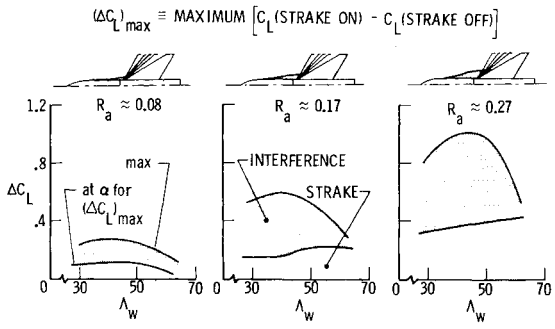

Fig. 9 Effect of strake span and wing sweep on $\Delta C_{L,max}$.

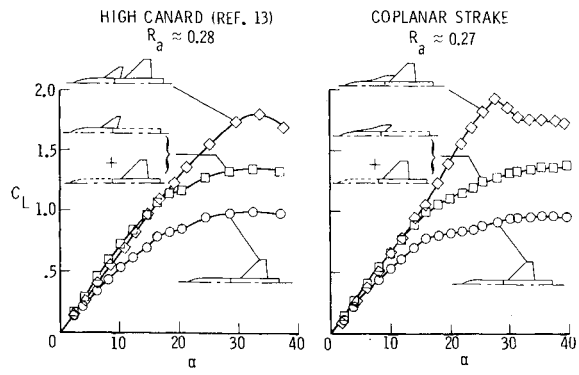

Fig. 10 Comparative example of an aerodynamic synergism, $\Lambda_w = 44$ deg.

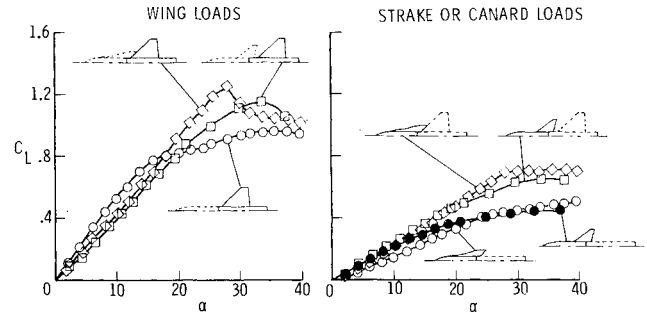

Fig. 11 Component loads for an aerodynamic synergism; high canard ($R_a \approx 0.28$), coplanar strake ($R_a \approx 0.27$), $\Lambda_w = 44$ deg.

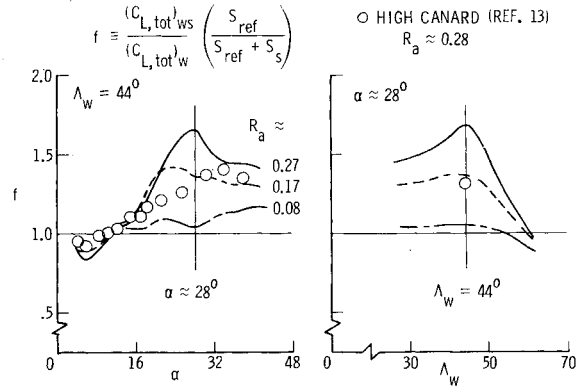

Fig. 12 Effect of planform and angle of attack on the additional lifting surface efficiency factor.

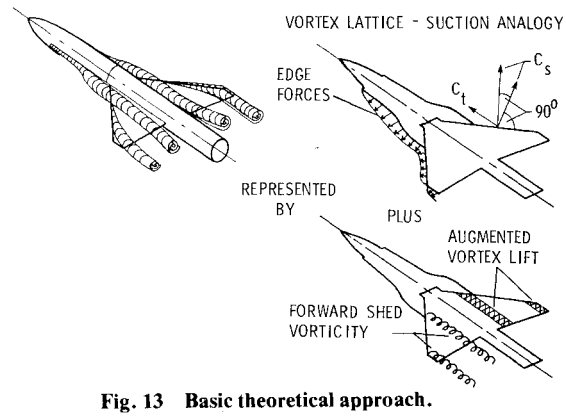

Fig. 13 Basic theoretical approach.

where $(C_{L,\text{tot}})_{ws}$ is the experimental total lift coefficient of a configuration with a strake (or canard), $(C_{L,\text{tot}})_w$ is the experimental total lift coefficient of the same configuration, but without the strake (or canard), S_a is the exposed area of the strake (or canard), and S_{ref} is the referenced area. Using the strake wing as an example, the parameter f will be unity if the increments in lift for the strake-on configurations divided by $(C_{L,\text{tot}})_w$ vary the same as the additional exposed area of the strake, S_s, divided by S_{ref}. The effects of planform and, for the 44 deg strake-wing configurations, α on f are presented in Fig. 12. Above approximately 16 deg, the addition of lifting surface in the form of a straked-wing geometry ($\Lambda_w = 44$ deg) can be seen to be an appreciably more efficient lifting surface concept ($f > 1$) due to the aforementioned interference effects, than the addition of lifting surface in the form of increased wing area ($f = 1$) would be. Similar calculations of f for the canard-wing configuration demonstrate that, for roughly the same amount of additional lifting surface, the strake wing is far more efficient at producing lift than is the close-coupled canard wing of Ref. 13. The right half of Fig. 12 presents a cross plot of sweep effects on f at an α of approximately 28 deg. Although the level of these results will depend upon α, the general trends with sweep angle shown are comparable to those for other α's. The decrease in f as the sweep angle exceeds 44 deg corresponds to the loss of interference lift such as was shown in Fig. 9 for $(\Delta C_L)_{\max}$. Even though the increments in lift for straked configurations incorporating the 60 deg wing might equally well be generated by appropriate increase in wing size ($f \approx 1$), the straked configurations may still be desirable since the strake represents a relatively light structure compared to the higher aspect-ratio wing or canard.

It should be recognized, of course, that trim limitations, lateral directional effects, and cruise drag increments also need to be taken into consideration when contrasting the various lifting surface concepts for practical application. Future strake-wing investigations incorporating wings designed for efficient cruise could be particularly useful in further evaluating this lifting surface concept. Additional parametric studies including the effect of wing leading-edge deflections as well as larger variations in strake planform would also be of interest.

Theoretical Analysis

An approach has been developed previously for the analysis of aerodynamic loads for configurations of complex planform, including the effects of separation-induced vortex flow.[16,17] This approach uses the vortex lattice method for the analysis of attached flow effects, the suction analogy of Polhamus for the analysis of separation-induced leading-edge vortex flow effects, and the method of Ref. 6 for the analysis of separation-induced side-edge vortex flow effects (Fig. 13). More recently, Lamar developed the concept of augmented vortex lift[7,8] as a means to quantify the effects of forward shed vorticity on aerodynamic lift estimates. This concept has proven useful for the analysis of simple wing planforms and could be applicable for the strake-wing configurations of the present investigation as well. Application of the theoretical approach is first presented for the component configurations, then for the complete strake-wing geometries.

Component Configurations

The augmented vortex lift concept was originally developed for wings which exhibited appreciable sweep differentials between the leading and side edges. These wings would develop distinct leading-edge and side-edge vortices and the augmented notion accounted for the shed vorticity of the leading-edge vortex over the aft portion of the lifting surface. However, the strakes of the present investigation exhibited very mild sweep differentials between the leading and side edges. The vorticity associated with these edges would, therefore, tend to be accumulative, resulting in one vortex being shed from the edges. Application of the augmented vortex lift concept to this flow situation would result in treating the strake much as an arrow wing. The augmented vortex lift would, therefore, be quantified as

$$K_{v,se} = \frac{(K_{v,le})_s + (K_{v,se})_s}{l_s}\,\tilde{c} \tag{2}$$

where l_s is the total length of the strake leading and side edges and $\tilde{c}$ is a characteristic length, which can be either positive or negative, over which the forward shed vorticity is assumed to persist. For a strake at low α, $\tilde{c}$ would be zero, but at high α, $\tilde{c}$ would be negative to reflect the loss of reattachment area and vortex lift due to the trailing-edge notching effect. Figure 14 illustrates the effect of angle of attack on the augmented vortex lift. Correlation with experiment demonstrates this method to provide reasonable estimates of the vortex lift developed by the isolated large strake ($\Lambda_{te,s} = 60$ deg) up to approximately 26 deg. Above this α, the data depart from the theory due to vortex breakdown effects. However, similar calculations for the isolated medium and small strakes ($\Lambda_{te,s} = 60$ deg) resulted in less accurate correlations with experiment at moderate α's (Fig. 15). The discrepancy between theory and experiment at these α's is most probably due to the flat plate representation of the fuselage. In addition to altering the edge force, the thick fuselage would tend to crowd the vortex off the strake itself at moderate to high α's. Additional oil flow studies, not presented herein, demonstrated the strake vortex to be displaced away from the strake upper surface so that it was acting more on the side of the fuselage for the small strake at moderate to high α's.

Complete Configuration

Surface flow patterns for the configuration incorporating the large strake and the 44 deg, wing are presented in Fig. 16. At $\alpha \approx 5$ deg, the strake and wing vortices are individually distinguishable and the strake vortex persists over the wing at

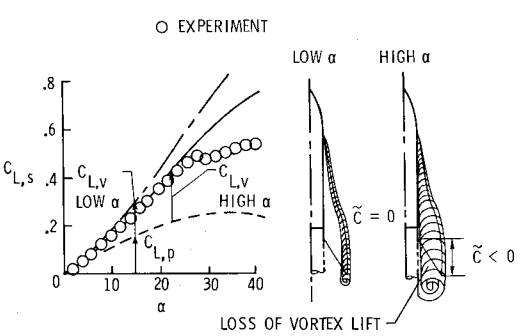

Fig. 14 Application of augmented vortex lift concept to an isolated strake configuration, $R_a \approx 0.27$, $\Lambda_{te,s} \approx 60$ deg.

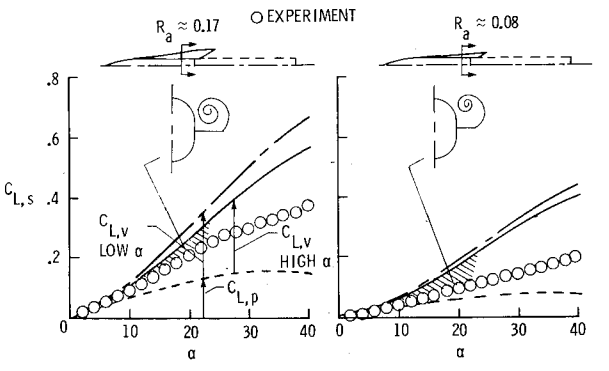

Fig. 15 Effect of span for isolated strake on lift correlation, $\Lambda_{te,s} \approx 60$ deg.

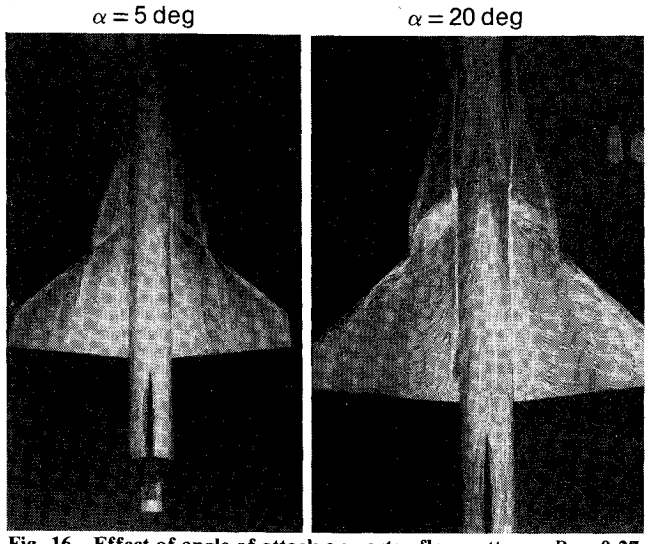

Fig. 16 Effect of angle of attack on vortex flow patterns, $R_a \approx 0.27$, $\Lambda_w = 44$ deg.

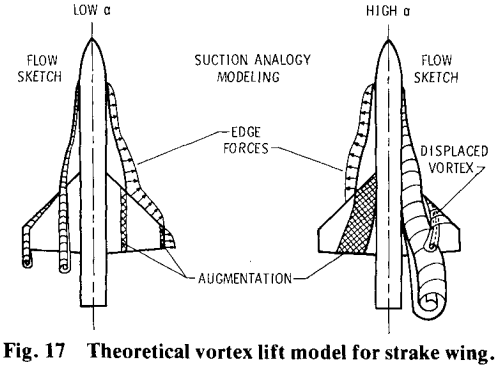

Fig. 17 Theoretical vortex lift model for strake wing.

a spanwise station near the tip of the strake. At $\alpha \approx 20$ deg, the wing surface flow pattern only evidences one large region of spanwise vortex flow which extends spanwise from the wing-fuselage juncture to roughly 86% of the reference wing span; outboard of this region the wing appears to be stalled. It is of interest to note that the cores of the strake vortices are visible as dark bands which curve outboard over the wing. The cores were observable due to naturally occurring condensation effects. Although the high-α flow patterns might be interpreted as an implication that the strake and wing vortices had coalesced into one, additional observations of the unburst wing leading-edge vortex core in addition to the strake core at these α's suggest that the wing vortex had not coalesced with the strake vortex, but merely had been displaced away from the wing upper surface by the strake vortex, thus, allowing the strake vortex to dominate the surface flow patterns. Accordingly, the vortex lift effects due to the wing leading- and side-edge vortices may be decreased at high α's due to vertical displacement.

The theoretical model of the vortex lift paramters for the strake-wing configurations is presented in Fig. 17. At low α's the augmented vortex lift for the strake itself will be zero, as had been the case for the isolated strake. Augmented effects will occur on the wing due to both the wing and strake vortices and may be expressed as:

$$(K_{v,se})_w = \frac{(K_{v,le})_w}{l_w}\tilde{c}_{\text{outbd},w} + \frac{(K_{v,le})_s + (K_{v,se})_s}{l_s}\tilde{c}_{\text{inbd},w} \qquad (3)$$

where l_w is the length of the exposed wing leading edge, $\tilde{c}_{\text{outbd},w}$ is the tip chord, and $\tilde{c}_{\text{inbd},w}$ is the wing chord at the strake wing juncture (Fig. 17). As α increases, the reattachment line moves inboard and an increasing amount of the strake vortex lift will be redistributed to the wing due to the sweep of the metric break. For the strake, this effect may be approximated in a limiting sense by utilizing the high-α definition of $\tilde{c}_s$ previously shown. To approximate the curved length over which the strake vortex persists on the wing, the chord at the wing fuselage juncture was chosen for $\tilde{c}_w$. The augmented effects at high α's may be expressed as:

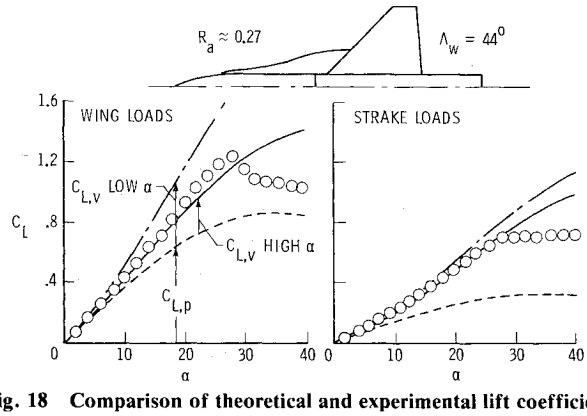

Fig. 18 Comparison of theoretical and experimental lift coefficients for a strake-wing configuration.

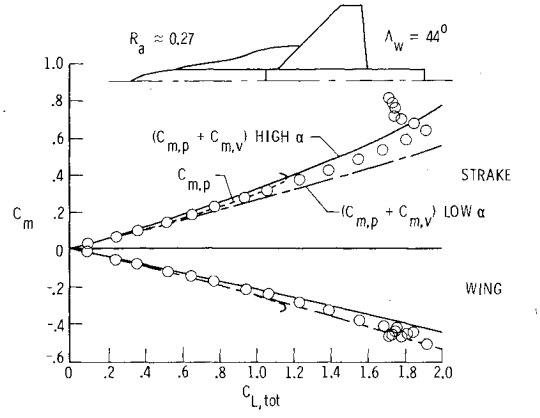

Fig. 19 Comparison of theoretical and experimental pitching moment coefficients for a strake-wing configuration.

$$(K_{v,se})_s = \frac{(K_{v,le})_s + (K_{v,se})_s}{l_s}\tilde{c}_s \qquad (4)$$

$$(K_{v,se})_w = \frac{(K_{v,le})_s + (K_{v,se})_s}{l_s}\tilde{c}_w \qquad (5)$$

Because vortex lift associated with the wing leading- and side-edge vortices may be decreased due to the aforementioned vertical displacement effects, one may assume

$$(K_{v,le})_w = (K_{v,se})_w = 0 \qquad (6)$$

as a limiting case.

Correlations between theoretical and experimental lift coefficients for the configuration incorporating the 44 deg wing and the large strake are presented in Fig. 18. The high-α vortex flow theory can be seen to provide a reasonable estimate of wing loads and an accurate estimate of strake loads up to an α where vortex breakdown occurs. Correlations between theoretical and experimental pitching moment characteristics (Fig. 19) show that the low- and high-α vortex flow theories bracket the data and provide reasonable estimates of experimental trends. Similar correlations were achieved at $M = 0.3$ for the other configurations incorporating either the medium or large strake.

The loads for the configurations incorporating the small strake were overestimated, as they had been with the wing off.

Concluding Remarks

The effects of parametric variations in strake span and wing sweep on the longitudinal aerodynamic characteristics of a general research model have been presented. Appreciable levels of lift have been shown to arise due to the mutually beneficial interference effects between the strake and the wing. Compared to a configuration incorporating a high canard and wing, the strake-wing configuration of roughly equivalent lifting surface area was found to develop higher levels of lift due to enhanced interference effects. Correlations between theory and experiment demonstrated that the suction analogy coupled with the augmented vortex lift concept provide reasonable estimates of the vortex flow aerodynamics for both component and total forces and moments up to high angles of attack.

References

[1] Luckring, J.M., "Subsonic Longitudinal and Lateral Aerodynamic Characteristics for a Systematic Series of Strake Wing Configurations," NASA TM X-78642, 1978.

[2] Fox Jr., C.H., "Subsonic Longitudinal and Lateral Directional Static Stability Characteristics of a General Research Fighter Model Employing a Strake-Wing Concept," NASA TM X-74071, 1978.

[3] Polhamus, E.C., "A Concept of the Vortex Lift of Sharp-Edge Delta Wings Based on a Leading-Edge-Suction Analogy," NASA TN D-3767, 1966.

[4] Polhamus, E.C., "Charts for Predicting the Subsonic Vortex-Lift Characteristics of Arrow, Delta, and Diamond Wings," NASA TN D-6243, 1971.

[5] Polhamus, E.C., "Predictions of Vortex-Lift Characteristics by a Leading-Edge Suction Analogy," *Journal of Aircraft*, Vol. 8, April 1971, pp. 193-199.

[6] Lamar, J.E., "Extension of Leading-Edge-Suction Analogy to Wings With Separated Flow Around the Side Edges at Subsonic Speeds," NASA TR R-428, 1974.

[7] Lamar, J.E., "Some Recent Applications of the Suction Analogy to Vortex-Lift Estimates," *Aerodynamic Analyses Requiring Advanced Computers*, Part II, NASA SP-347, 1975, pp. 985-1011.

[8] Lamar, J.E., "Summary of Some Recent Studies of Subsonic Vortex Lift and Parameters Affecting the Leading-Edge Vortex Stability," AIAA Paper 76-414, San Diego, Calif., July 1976.

[9] McKinney, L.W. and Dollyhigh, S.M., "Some Trim Drag Considerations for Maneuvering Aircraft," *Journal of Aircraft*, Vol. 8, Aug. 1971, pp. 623-629.

[10] Dollyhigh, S.M., "Static Longitudinal Aerodynamic Characteristics of Close-Coupled Wing-Canard Configurations at Mach Numbers From 1.60 to 2.86," NASA TN D-6597, 1971.

[11] Gloss, B.B. and McKinney, L.W., "Canard-Wing Lift Interference Related to Maneuvering Aircraft at Subsonic Speeds," NASA TM X-2897, 1973.

[12] Gloss, B.B., "Effect of Canard Height and Size on Canard-Wing Interference and Aerodynamic Center Shift Related to Maneuvering Aircraft at Transonic Speeds," NASA TN D-7505, 1974.

[13] Gloss, B.B., "The Effect of Canard Leading-Edge Sweep and Dihedral Angle of the Longitudinal and Lateral Aerodynamic Characteristics of a Close-Coupled Canard Wing Configuration," NASA TN D-7814, 1974.

[14] Gloss, B.B., "Effect of Wing Planform and Canard Location and Geometry on the Longitudinal Aerodynamic Characteristics of a Closed-Coupled Canard Wing Model at Subsonic Speeds," NASA TN D-7910, 1975.

[15] Gloss, B.B., Henderson, W.P., and Huffman, J.K., "Effect of Canard Position and Wing Leading-Edge Flap Deflection on Wing Buffet at Transonic Speeds," NASA TM X-72681, 1975.

[16] Margason, R.J. and Lamar, J.E., "Vortex-Lattice FORTRAN Program for Estimating Subsonic Aerodynamic Characteristics of Complex Planforms," NASA TN D-6142, 1971.

[17] Lamar, J.E. and Gloss, B.B., "Subsonic Aerodynamic Characteristics of Interacting Lifting Surface with Separated Flow Around Sharp Edges Predicted by a Vortex-Lattice Method," NASA TN D-7921, 1975.